Int. J. Heat Mass Transfer. Vol. 18, pp. 363–380. Pergamon Press 1975. Printed in Great Britain

THERMAL PERFORMANCE CHARACTERISTICS OF HEAT PIPES

K. H. SUN* and C. L. TIEN
Department of Mechanical Engineering, University of California, Berkeley, California, U.S.A.

(*Received* 15 *February* 1974 *and in revised form* 27 *June* 1974)

Abstract—Theoretical and experimental studies are conducted to evaluate the overall thermal performance of single-component and gas-loaded heat pipes. In the analysis, the simple conduction model developed recently for the single-component heat pipes has been extended to predict the wall temperature profiles of gas-loaded heat pipes with phase change occurring in the evaporator wick. Experimental evaluation of the thermal performance is made with two working fluids (water and acetone) under two corresponding sink environments (boiling water and boiling alcohol). The heat pipe system is designed with variable-length heat input and output sections under a wide range of heat input conditions. Measured results agree well with theoretical predictions.

NOMENCLATURE

Bi, Biot number with respect to wick, defined in equation (1);
D_o, O.D. of the heat pipe;
D_i, I.D. of the heat pipe;
D_v, diameter of the vapor core inside the heat pipe;
H, dimensionless parameter defined in equation (10);
h, heat-transfer coefficient between the pipe wall and the ambient;
h_e, effective film coefficient for the wick of the heat input section;
k_i, k_w, thermal conductivity of liquid–wick matrix and pipe wall, respectively;
L, total length of heat pipe;
L_a, L_e, length of the adiabatic and heat input sections, respectively;
L_c, length of the heat output section for single-component heat pipes or length of the condenser part of the heat output section for the gas-loaded heat pipes;
L_g, length of the non-condensible gas region defined in equation (36);
M, dimensionless parameter, defined in equation (2);
N, total number of moles of the non-condensible gas;
P_g, partial pressure of the non-condensible gas;
P_{gL}, partial pressure of the non-condensible gas at the condenser end;
Q, rate of heat input to the heat pipe;
R_u, universal gas constant;
T_g, temperature of the non-condensible gas;
T_{gL}, temperature of the non-condensible gas at the condenser end;
T_0, ambient sink temperature;
T_s, temperature of saturated vapor;
T_w, temperature of pipe wall;
$\bar{T}_{wc}$, mean wall temperature at the heat output section;
V, volume of the vapor and gas;
x, y, z, v, axial coordinate for the heat input, adiabatic, condenser part of the heat output and non-condensible region, respectively.

Greek symbols

β, dimensionless length coordinate for the adiabatic section, defined as y/L;
β_a, dimensionless length for the adiabatic section, defined as L_a/L;
η, dimensionless length coordinate for the heat input section, defined as x/L;
η_e, dimensionless length for the heat input section, defined as L_e/L;
θ_0, dimensionless saturated vapor temperature, defined in equation (3);
θ_1, dimensionless wall temperature at the junction of heat input and adiabatic sections;
θ_2, dimensionless wall temperature at the junction of adiabatic and condenser part of heat output section;
θ_3, dimensionless wall temperature at the fictitious junction of condenser and non-condensible gas region;

*Now, Senior Engineer, Nuclear Energy Division, General Electric Company, San Jose, California, U.S.A.

θ_a, dimensionless wall temperature at the adiabatic section, defined in equation (5);
θ_c, dimensionless wall temperature at the heat output section, defined in equation (6), or at the condenser part of the heat output section;
θ_e, dimensionless wall temperature at the heat input section, defined in equation (4);
θ_g, dimensionless wall temperature at the non-condensible gas region, defined in equation (19);
λ, dimensionless length coordinate for the non-condensible gas region, defined as v/L;
λ_g, dimensionless length of the non-condensible gas region, defined as L_g/L;
ξ, dimensionless length coordinate for the heat output section for single-component heat pipes, or for the condenser part of the heat output section for gas-loaded heat pipes, defined as z/L;
ξ_c, dimensionless length of the heat output section for single-component heat pipes, or of the condenser part of the heat output section for gas-loaded heat pipes, defined as L_c/L.

Subscripts

a, refers to adiabatic section;
c, refers to heat output section for single-component heat pipes or condenser part of heat output section for gas-loaded heat pipes;
e, refers to heat input section;
g, refers to non-condensible gas region;
i, refers to wick (except D_i);
w, refers to pipe wall.

INTRODUCTION

THE OPERATING characteristics of a heat pipe have been the subject of extensive studies in the development of heat pipe technology [1–3]. However, most of these studies were focused on the hydrodynamic and thermal behaviors in certain portions of the heat pipe, such as evaporator, condenser, vapor zone, wick, etc. Little attention has been given to the overall performance by considering the heat pipe as a whole, including, for instance, the axial conduction along the pipe wall and the heat-transfer mode in the source and sink regions.

Recently, a simple conduction model was developed for heat pipe thermal performance [4]. With the consideration of the interactions of axial heat conduction along the pipe wall with various transport processes inside and outside the heat pipe, the model leads to the prediction of the vapor temperature, the axial wall temperature profile and the axial mass flow distribution of a single-component heat pipe operating in steady state. It was shown that the prediction of overall thermal performance could only be made by combining the conduction model with an enclosure condition which is a unique characteristic of the heat pipe.

The enclosure condition is based on the fact that the heat pipe is a closed system. During the steady state there are no mass and energy accumulations. The vapor temperature will adjust according to the heat input and ambient conditions so that the condensing mass rate is equal to the evaporating mass rate, and all the heat input is rejected to the ambient. In short, the enclosure condition accounts for the overall energy and mass balances of the heat pipe system, while the conduction model deals only with the local heat flux and mass flow rate.

The analysis derived from the simple conduction model shows that the thermal performance of a heat pipe is greatly influenced by two dimensionless parameters, Bi and M, where

$$Bi \equiv \frac{hD_0}{2k_i}\ln(D_i/D_v) \tag{1}$$

and

$$M \equiv \left[\frac{8k_i L^2}{k_w(D_0^2-D_i^2)\ln(D_i/D_v)}\right]^{1/2}. \tag{2}$$

The parameter Bi characterizes the heat removing mechanism at the condenser ambient, while M governs the effect of axial conduction along the pipe wall. The effect of axial conduction becomes more dominant at smaller values of M.

The results of the analysis lead to the conclusion that the heat pipe effectiveness and the capillary pumping limited heat-transfer rate can be improved by increasing axial wall conduction. However, to increase axial conduction does not mean primarily to increase the direct heat transfer from the evaporator to the condenser along the pipe wall, but to decrease the thermal resistance across the wick.

The conduction model has been applied only to single-component heat pipes. Analytical prediction for the gas-loaded heat pipe is restricted to the vicinity of the vapor–gas interface [5]. The purpose of the present study is to extend the conduction-model analysis to include the effect of phase change inside the evaporator wick and the effect of non-condensible gas in the heat output section of the heat pipe, and to determine experimentally the effects of various parameters for comparison with theoretical predictions.

THE EFFECT OF PHASE CHANGE IN THE EVAPORATOR WICK

In the analysis of the simple conduction model [4], it is assumed that the thermal conductance of the evaporator wick is the same as that of the condenser wick. This assumption is supported by the experimental results of Sockalingam [6] and Ferrell *et al.* [7], but the results by Seban and Abhat [8] and Corman [9] indicate otherwise. The reason for this discrepancy is difficult to ascertain, and will be discussed later.

Assuming that the radial heat transfer in the evaporator wick can be characterized by an effective wick film coefficient, h_e, the radial heat flux based on the inner pipe surface is represented by $h_e(T_{we}-T_s)$. The conduction model can be modified to account for the case of phase change occurring inside the evaporator wick, provided that: $h_e D_i/2k_w \ll 1$. By following the same analysis given in [4] the axial wall temperature profile and the vapor temperature can be predicted based on the same coordinate system which is reproduced in Fig. 1 for convenience.

The dimensionless vapor temperature

$$\theta_0 \equiv \frac{T_0-T_s}{(Q/2\pi L_e k_i)\ln(D_i/D_v)} = \frac{-\dfrac{\eta_e}{Bi}-\dfrac{a_3b_1\gamma_5}{\gamma_6\Delta M(1+Bi)^{1/2}}}{\dfrac{\xi_c}{1+Bi}+\dfrac{\gamma_5 Bi}{\gamma_6 M(1+Bi)^{3/2}}-\dfrac{a_1b_3\gamma_5}{\gamma_6\Delta M(1+Bi)^{1/2}}}. \quad (3)$$

The dimensionless wall temperatures

For the heat input section, $0 \leqslant x \leqslant L_e$, $0 \leqslant \eta \leqslant \eta_e$

$$\theta_e(\eta) \equiv \frac{T_{we}(x)-T_s}{(Q/2\pi L_e k_i)\ln(D_i/D_v)} = \frac{1}{H}-\left(\frac{1}{H}-\theta_1\right)\frac{\cosh MH^{1/2}\eta}{\gamma_2}. \quad (4)$$

For the adiabatic section, $0 \leqslant y \leqslant L_a$, $0 \leqslant \beta \leqslant \beta_a$

$$\theta_a(\beta) \equiv \frac{T_{wa}(y)-T_s}{(Q/2\pi L_e k_i)\ln(D_i/D_v)} = \theta_1\cosh M\beta+(\theta_2-\theta_1\gamma_4)\frac{\sinh M\beta}{\gamma_3}. \quad (5)$$

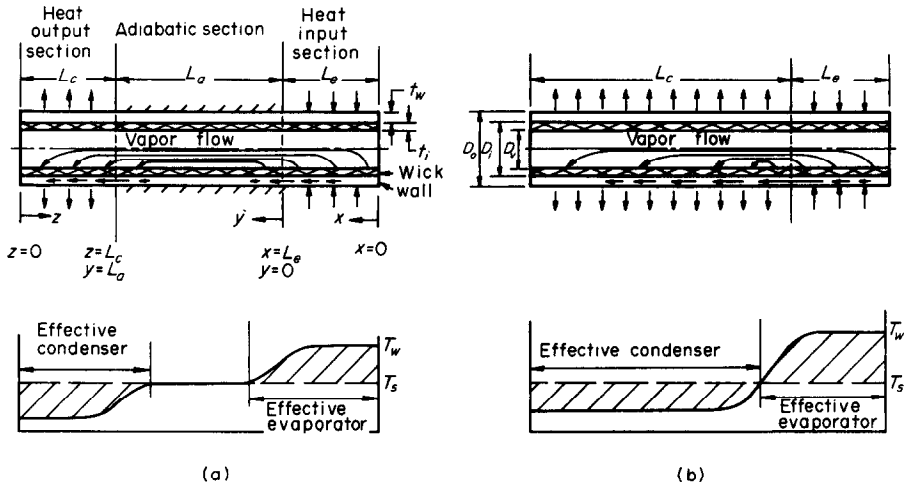

FIG. 1. Axial wall temperature variations along the heat pipe.

For the heat output section, $0 \leqslant z \leqslant L_c$, $0 \leqslant \xi \leqslant \xi_c$

$$\theta_c(\xi) \equiv \frac{T_{wc}(z)-T_s}{(Q/2\pi L_e k_i)\ln(D_i/D_v)} = \frac{Bi\theta_0}{1+Bi}+\left(\theta_2-\frac{Bi\theta_0}{1+Bi}\right)\frac{\cosh M(1+Bi)^{1/2}\xi}{\gamma_6} \quad (6)$$

where

$$\theta_1 \equiv \frac{a_3b_2-a_2b_3\theta_0}{\Delta}, \quad \theta_2 \equiv \frac{a_1b_3\theta_0-a_3b_1}{\Delta} \quad (7)$$

$$\Delta \equiv a_1b_2-a_2b_1$$

$$a_1 \equiv \gamma_4+\frac{\gamma_1\gamma_3H^{1/2}}{\gamma_2}, \quad a_2 \equiv -1,$$

$$a_3 \equiv \frac{\gamma_1\gamma_3}{\gamma_2H^{1/2}} \quad (8)$$

$$b_1 \equiv -\frac{1}{\gamma_3}, \quad b_2 \equiv \frac{\gamma_4}{\gamma_3} + \frac{\gamma_5(1+Bi)^{1/2}}{\gamma_6},$$

$$b_3 \equiv \frac{\gamma_5 Bi}{\gamma_6(1+Bi)^{1/2}}$$

$$\gamma_1 \equiv \sinh MH^{1/2}\eta_e, \qquad \gamma_2 \equiv \cosh MH^{1/2}\eta_e$$
$$\gamma_3 \equiv \sinh M\beta_a, \qquad \gamma_4 \equiv \cosh M\beta_a \tag{9}$$
$$\gamma_5 \equiv \sinh M(1+Bi)^{1/2}\xi_c, \quad \gamma_6 \equiv \cosh M(1+Bi)^{1/2}\xi_c$$

$$\eta_e \equiv \frac{L_e}{L}, \quad \beta_a \equiv \frac{L_a}{L}, \quad \xi_c \equiv \frac{L_c}{L}$$

and

$$H \equiv \frac{h_e D_i}{2k_i}\ln(D_i/D_v). \tag{10}$$

With the vapor temperature and wall temperature known, the local radial heat flux and the axial mass flow distribution can be calculated easily. The dimensionless parameter H compares the effective film coefficient of the evaporator wick with that of pure conduction. For $H = 1$, the above equations reduce to the corresponding results derived before [4]. In this case, the enclosure condition can be illustrated in Fig. 1 that the shaded area above the vapor temperature is equal to that beneath it. The major difference between the present case with phase change in the evaporator wick and the conduction model, is the temperature drop across the evaporator. For $H > 1$, the thermal resistance of the evaporator wick is smaller than the conduction resistance. Therefore, the overall thermal effectiveness is higher. This means that in Fig. 1 the shaded area above the vapor temperature is smaller than the area beneath it.

The present analysis predicts the wall temperature of a heat pipe operating normally with phase change occurring inside the evaporator wick. The parameter H which characterized the phase change phenomenon is generally not known and is to be determined from experimental results.

THERMAL PERFORMANCE OF GAS-LOADED HEAT PIPES

Calculation of wall temperature profiles

In the model development for predicting the thermal performance of gas-loaded heat pipes, the wall temperature profile in the vicinity of the vapor–gas front is predicted by solving the mass diffusion and heat-conduction equations simultaneously [5, 10, 11]. The analysis predicts the overall wall temperature profile very well for heat pipes operating with a small external condenser heat-transfer coefficient, such as those operating with heat rejection by radiation of free convection. However, for heat pipes operating with two end portions in contact with solid bodies, or for those operating in an ambient with large external condenser heat-transfer coefficient, such as boiling, the temperature drop across the wick is comparable with that between the pipe and the ambient. The analysis becomes inapplicable since it does not take into account the heat-transfer process across the evaporator wick. The difference of the wall temperature profiles for these two cases is illustrated in Fig. 2.

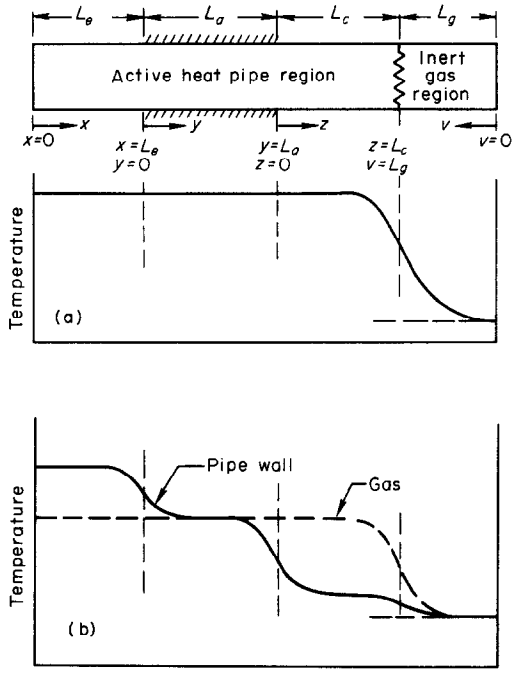

FIG. 2. The typical temperature profiles of the pipe wall and gas-loaded heat pipe. (a) External condenser heat-transfer coefficient, small ($h = 0(10^{-3})$W/cm^2 °K). (b) External condenser heat-transfer coefficient, large ($h = 0(10^{-1})$W/cm^2 °K).

In the present analysis, the simple conduction model is used as a basis to predict the wall temperature profile. The diffusion process is neglected since it is only of secondary importance in establishing the steady-state wall temperature profile [5]. To characterize the effect of non-condensible gas, a dimensionless length similar to the flat-front model, is defined and incorporated into the conduction model.

The formulation of the problem is similar to that in the simple conduction model [4]. For the non-condensible gas region, the vapor temperature is assumed to be the same as the wall temperature with no radial heat flux across the wick. Heat-conduction equations are first set up for the four sections (heat input, adiabatic, condenser region of the heat output, and non-condensible gas region of the heat output) with the condition of temperature and heat flux

continuity prescribed at their junctions. The coordinate system is given in Fig. 2.

Based on the cylindrical differential elements, dx, dy, dz and dv, in each heat pipe section, simple heat balance consideration leads to the following governing equations and boundary conditions in dimensionless forms: for the heat input section, $0 \leqslant x \leqslant L_e$

$$\theta_e''(\eta) - M^2 H \theta_e(\eta) + M^2 = 0 \tag{11}$$

$$\theta_e'(0) = 0, \quad \theta_e(\eta) = \theta_1 \tag{12}$$

in which the dimensionless parameter H characterizes the effect of phase change inside the wick, for the adiabatic section, $0 \leqslant y \leqslant L_a$

$$\theta_a''(\beta) - M^2 \theta_a(\beta) = 0 \tag{13}$$

$$\theta_a(0) = \theta_1, \quad \theta_a(\beta_a) = \theta_2 \tag{14}$$

for the condenser region of the heat output section, $0 \leqslant z \leqslant L_c$

$$\theta_c''(\xi) - M^2(1+Bi)\theta_c(\xi) + M^2 Bi \theta_0 = 0 \tag{15}$$

$$\theta_c(0) = \theta_2, \quad \theta_c(\xi_c) = \theta_3 \tag{16}$$

for the non-condensible gas region of the heat output section, $0 \leqslant v \leqslant I_g$

$$\theta_g''(\lambda) - M^2 Bi \theta_g(\lambda) + M^2 Bi \theta_0 = 0 \tag{17}$$

$$\theta_g'(0) = 0, \quad \theta_g(\lambda_g) = \theta_3 \tag{18}$$

where,

$$\theta_g(\lambda) \equiv \frac{T_{wv}(v) - T_s}{(Q/2\pi L_e k_i)\ln(D_i/D_v)}, \quad \lambda_g \equiv L_g/L \tag{19}$$

and, the heat flux continuity relation

$$\begin{aligned} \theta_e'(\eta_e) &= \theta_a'(0) \\ \theta_a'(\beta_a) &= \theta_c'(0) \\ \theta_c'(\xi_c) + \theta_g'(\lambda_g) &= 0. \end{aligned} \tag{20}$$

Solutions for the dimensionless wall temperature in each section can be obtained through simple mathematical manipulations. They are for $0 \leqslant \eta \leqslant \eta_e$

$$\theta_e(\eta) = \frac{1}{H} - \left(\frac{1}{H} - \theta_1\right)\frac{\cosh M(H)^{1/2}\eta}{\gamma_2} \tag{21}$$

for $0 \leqslant \beta \leqslant \beta_a$

$$\theta_a(\beta) = \theta_1 \cosh M\beta + (\theta_2 - \theta_1\gamma_4)\frac{\sinh M\beta}{\gamma_3} \tag{22}$$

for $0 \leqslant \xi \leqslant \xi_c$

$$\theta_c(\xi) = \frac{Bi\theta_0}{1+Bi} + \left(\theta_2 - \frac{Bi\theta_0}{1+Bi}\right)\cosh M(1+Bi)^{1/2}\xi + \left[\theta_3 - \frac{Bi\theta_0}{1+Bi} - \left(\theta_2 - \frac{Bi\theta_0}{1+Bi}\right)\gamma_6\right] \times \frac{\sinh M(1+Bi)^{1/2}\xi}{\gamma_5} \tag{23}$$

for $0 \leqslant \lambda \leqslant \lambda_g$

$$\theta_g(\lambda) = (\theta_3 - \theta_0)\frac{\cosh M(Bi)^{1/2}\lambda}{\gamma_8} + \theta_0 \tag{24}$$

where

$$\begin{aligned} \gamma_7 &\equiv \sinh M(Bi)^{1/2}\lambda_g \\ \gamma_8 &\equiv \cosh M(Bi)^{1/2}\lambda_g. \end{aligned}$$

Combining equations (21)–(24) with equation (20), there results the following expression for θ_1, θ_2 and θ_3:

$$\theta_1 = \frac{A_4\alpha_2 - A_2\alpha_3\theta_0}{\alpha_1} \tag{25}$$

$$\theta_2 = \frac{A_1\alpha_3\theta_0 - A_4B_1C_3}{\alpha_1} \tag{26}$$

and

$$\theta_3 = \frac{(A_1\alpha_4 - A_2B_1C_4)\theta_0 + A_4B_1C_2}{\alpha_1} \tag{27}$$

where

$$\begin{aligned} \alpha_1 &\equiv A_1\alpha_2 - A_2B_1C_3 \\ \alpha_2 &\equiv B_2C_3 - B_3C_2 \\ \alpha_3 &\equiv B_4C_3 - B_3C_4 \\ \alpha_4 &\equiv B_2C_4 - B_4C_2 \end{aligned} \tag{28}$$

$$\begin{aligned} A_1 &\equiv M\left(\frac{H^{1/2}\gamma_1}{\gamma_2} + \frac{\gamma_4}{\gamma_3}\right) \\ A_2 &\equiv -\frac{M}{\gamma_3} \\ A_4 &\equiv \frac{M\gamma_1}{H^{1/2}\gamma_2} \\ B_1 &\equiv A_2 \\ B_2 &\equiv \frac{M\gamma_4}{\gamma_3} + \frac{\gamma_6 M(1+Bi)^{1/2}}{\gamma_5} \\ B_3 &\equiv -\frac{M(1+Bi)^{1/2}}{\gamma_5} \\ B_4 &\equiv \frac{(\gamma_6 - 1)MBi}{\gamma_5(1+Bi)^{1/2}} \\ C_2 &\equiv B_3 \\ C_3 &\equiv M\left[\frac{(1+Bi)^{1/2}\gamma_6}{\gamma_5} + \frac{(Bi)^{1/2}\gamma_7}{\gamma_8}\right] \\ C_4 &\equiv B_4 + \frac{M(Bi)^{1/2}\gamma_7}{\gamma_8}. \end{aligned} \tag{29}$$

It is noted that the dimensionless vapor temperature θ_0 is still unknown, yet to be determined by the enclosure condition which can be expressed in the dimensionless form

$$\int_0^{\xi_c} \theta_c(\xi)\,d\xi + \int_0^{\lambda_g} \theta_g(\lambda)\,d\lambda = \frac{\eta_e}{Bi} + \theta_0(\xi_c + \lambda_g). \tag{30}$$

Combining the above equation with equations (23), (24) and (26) and (27) yields the following expression for θ_0.

$$\theta_0 = \frac{\dfrac{\eta_e}{Bi} + \dfrac{A_4 B_1}{\alpha_1}(C_3 D_2 - C_2 D_3)}{-D_1 + \dfrac{1}{\alpha_1}(A_1\alpha_3 D_2 + A_1\alpha_4 D_3 - A_2 B_1 C_4 D_3)} \quad (31)$$

where

$$D_1 \equiv \frac{\xi_c}{1+Bi} + \frac{\gamma_7}{\gamma_8 M(Bi)^{1/2}} + \frac{2B_4}{M^2(1+Bi)}$$
$$D_2 \equiv \frac{B_4}{M^2 Bi} \quad (32)$$
$$D_3 \equiv \frac{C_4}{M^2 Bi}$$

or in the functional form

$$\theta_0 = \theta_0(\eta_e, \beta_a, \xi_c, \lambda_g, M, Bi, H). \quad (33)$$

With known values of the dimensionless parameters which appear in equation (33), θ_0 can be calculated without difficulty. Substituting the value of θ_0 into equations (25)–(27) determines θ_1, θ_2 and θ_3. With θ_0, θ_1, θ_2 and θ_3 known, the dimensionless wall temperature can be calculated. However, among these parameters, the dimensionless length for the non-condensible gas region, λ_g, is yet to be defined.

The length of the non-condensible gas section

The present analysis for the gas-loaded heat pipe was based on the assumption that a sharp interface exists between the vapor of the working fluid and the non-condensible gas. While a flat-front interface does not exist in the actual case, the length to characterize the non-condensible gas region needs to be properly defined.

For an ideal gas mixture, the number of moles of the non-condensible gas in a differential element of pipe volume is simply [11]

$$dn = \frac{P_g dV}{R_u T_g} = \frac{P_g A_v}{R_u T_g} dL \quad (34)$$

where P_g and T_g are the partial pressure and the temperature of the gas in the element dV. While the total mass, or the number of moles, for a given heat pipe remains invariant for all operating conditions, the integration of equation (34) over the whole heat pipe length is a constant, i.e.

$$N = \frac{A_v}{R_u}\int_0^L \frac{P_g}{T_g} dL. \quad (35)$$

Using the partial pressure and the temperature of the gas at the condenser end, P_{gL} and T_{gL} as reference, the length for the non-condensible gas region can be defined as

$$L_g \equiv \frac{R_u T_{gL} N}{A_v P_{gL}} = \frac{T_{gL}}{P_{gL}}\int_0^L \frac{P_g}{T_g} dL \quad (36)$$

and L_g is illustrated in Fig. 3.

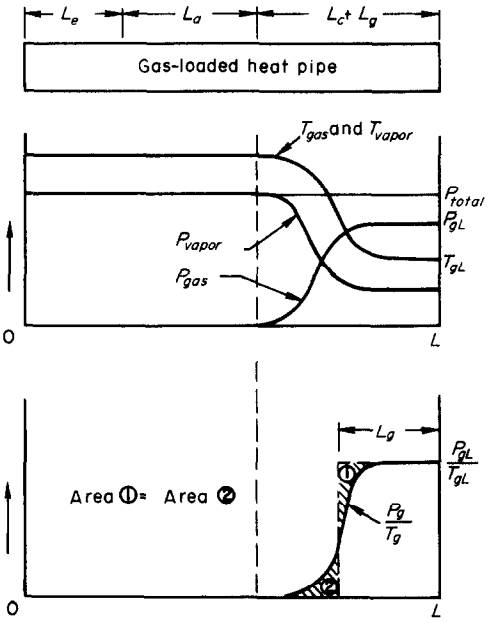

FIG. 3. Figurative illustration for the definition of length for the non-condensible gas region, L_g.

The values of P_{gL} and T_{gL}, which are dependent upon the system parameters as well as the operating conditions of the heat pipe, can be obtained from the experimental data: T_{gL} from the gas temperature at the condenser end, and P_{gL} from the difference of the total pressure of the heat pipe and the vapor saturation pressure corresponding to the temperature T_{gL}. While the total pressure is the pressure of the pure saturated vapor, an additional measurement of vapor temperature at the evaporator end will be sufficient to determine L_g.

The definition of L_g is more representative of the actual case when the vapor–gas interface is sharper. Physically, this corresponds to the case of low vapor pressure at sink temperature, large slope of the vapor pressure curve (i.e. large gas-control sensitivity factor [11]), and minimum axial conduction.

Later, the values of L_g are evaluated for the gas-loaded water heat pipes operating under different heat input levels and with different amounts of non-condensible gas. It will be shown that by incorporating the values of L_g into the conduction model, the wall temperature profiles can be predicted.

EXPERIMENT

Apparatus

A well-instrumented heat pipe system shown in Fig. 4 was designed and constructed to provide experimental evidence to assess and confirm the present analysis. The design information was fully described in [12].

The heat pipe was a copper tube 2-ft long and 0·875-in in O.D. with 0·065-in thick wall. The heat input section was wrapped by ceramic-coated nichrome heaters which covered a length of 7·5-in in five

The wicking material used in the experiment was sintered nickel fibers with porosity 0·80. This material was manufactured in rectangular sheets of about 12-in long. For the present experiment, a wick of 24-in long was made by overlapping and sewing a 0·5-in long piece on two 12-in long pieces. Wick rise tests were performed on both wicks with and without overlapping to check the effect of overlapping on the wick capillary pumping characteristics. The results showed that it exerted little influence on the equilibrium pumping

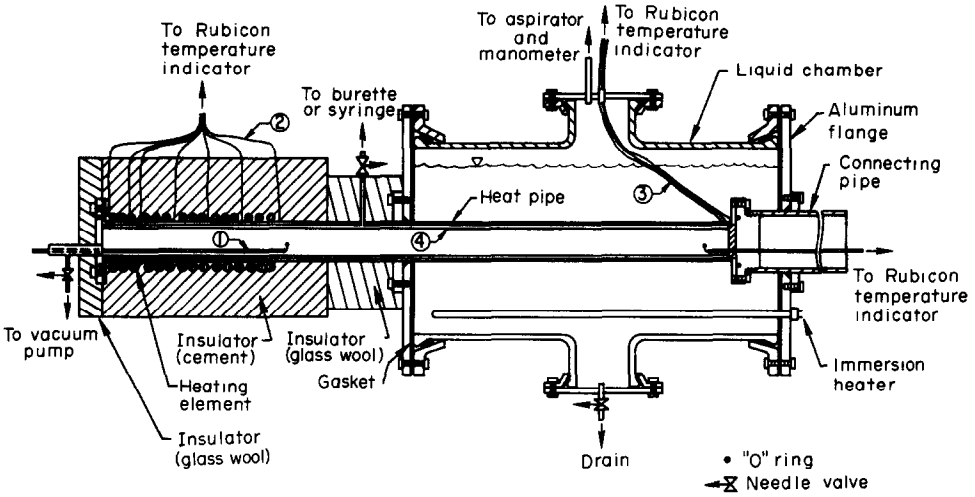

FIG. 4. The heat pipe assembly. 1. Two thermocouples shielded by stainless steel tube. 2. Seven point-soldered thermocouples. 3. Eight thermocouples imbedded in grooves. 4. Sintered nickel fiber wick.

circuits, so that the length of the heat input section could be varied five-fold. The heat output section was completely immersed in a cross-shaped glass liquid chamber attached to the heat pipe by aluminum flanges. The liquid chamber could be moved along the heat pipe to vary the length of the heat output section. An immersion heater made of nichrome heaters was inserted in the liquid chamber which was connected to an aspirator, so that, by setting the preheater power and the chamber pressure, the ambient condition of the heat output section could be adjusted. The possible large variation of the length of the heat input and output sections provided great flexibility for adjusting heat pipe system parameters.

The heat pipe was instrumented with fifteen thermocouples along the pipe wall and two thermocouples inserted into the interior of the heat pipe through the end flanges for vapor temperature measurement. The one through the evaporator end flange could be moved longitudinally during the test to measure the vapor and gas temperature at different axial positions.

heights, although the one with overlapping required somewhat longer time to reach the equilibrium level. This indicated that the overlapping did not impose a discontinuity on the liquid flow through the wick. To install the wick into the heat pipe, the wick was mounted on a wooden mandrel forming two layers and forced to fit tightly against the inner pipe wall. By excluding the region of wick overlapping which occupied only 2 per cent of the pipe length, the mean diameter of the vapor core was measured to be 0·600 in with a deviation of ± 7 per cent. Since the region of wick overlapping was always in the adiabatic section of the heat pipe, its effect on the overall thermal performance was virtually negligible.

A vacuum pump was connected to the heat pipe through the brass flanges at the evaporator end. The filling line for the heat pipe was a 0·25-in dia. brass tube brazed at the location 8·8 in from the evaporator end. During the operation, the heat input and adiabatic sections of the heat pipe were completely insulated. A piece of teflon was plugged into the pipe condenser end

to prevent vapor from direct contact with the end flange. The heat loss was estimated to be negligible through the condenser end, and at most 4·5 per cent through the evaporator end.

Procedure

Prior to the assembly, the pipe, the wicking material, and the mandrel were thoroughly cleaned. The cleaning process included washing by detergent and rinsing by hot water repeatedly several times. After drying, the inside of the pipe was repeatedly wiped by cloth soaked with acetone while the wick was dipped in an acetone pool for several hours. After the cleaning process, the heat pipe was assembled and evacuated for twenty-four hours.

For the filling of heat pipe, the working fluid (distilled water and reagent-grade acetone) contained in a burette was allowed to flow into the pipe slowly (about 0·1 cm^3/s) while the pipe was under vacuum. Before the filling, the water was boiled for three hours to exclude dissolved gas. For the test of gas-loaded heat pipes, an additional amount of air was injected into the pipe with a syringe.

When the system was ready for operation, the power to the evaporator heater and the immersion heater was turned on. The temperatures of the liquid in the glass chamber and evaporator wall were constantly monitored. When the liquid reached the saturation temperature, the power to the immersion heater was turned down merely to maintain it at the saturation point. Steady-state was determined when the increment of the evaporator wall temperature was less than 0·1°C in 10 min. When steady-state was reached, the heat input to the evaporator heater, the wall and vapor temperatures were recorded.

Extremely careful precautions were taken to prevent the existence of non-condensible gas in the tests of single-component heat pipes. Besides evacuating the system by a vacuum pump and boiling the working fluid before the filling process, the vapor temperatures near the two end flanges of the heat pipe were constantly checked. During the normal single-component test, they differed within 0·5°C due to the fin effect. In some cases after the heat pipe having been operated for several hours, the difference increased to 2°C. This was first thought to be caused by the superheating and subcooling of the vapor at the evaporator and the condenser. However, by opening the condenser end flange slightly, vapor was noticed gushing out of the pipe, and the temperature difference suddenly returned to normal. Therefore, it was believed that the existence of non-condensible gas was the cause of the excessive temperature drop. The non-condensible gas could either be dissolved from the working fluid or trapped in the wick before the operation. During the single-component test, the test was immediately terminated when the difference of the vapor temperatures measured near the two ends of heat pipe was noted to exceed 1°C. After the heat pipe had undergone the purging process, the test was continued. Before each test of gas-loaded heat pipes, the heat pipe was kept in an operating condition for several hours during which the condenser end flange was opened several times to purge out the possible existence of the non-condensible gas. Then, the power was turned off and the heat pipe was cooled down while the thermocouples in the vapor region were constantly monitored. When the temperature dropped below the saturation temperature corresponding to the atmospheric condition, a prescribed amount of air, which was contained in the syringe connected to the filling line, was allowed into the heat pipe. Thus, the gas-loaded heat pipe was ready for testing.

Measurements

There were fifteen test runs conducted in the experimental program. Runs 1 to 7 were single-component tests in four different arrangements of heat pipe geometry. Runs 8 to 15 were gas-loaded tests with the geometry fixed while data were taken at four levels of heat input and with the amount of non-condensible gas prescribed at 10, 30, 50 and 70 cm^3. Water and acetone were used as the working fluids of the heat pipe. Air was employed through the gas-loaded tests as the non-condensible gas. Water and alcohol were chosen to be the liquid in the heat output sink for the water and acetone tests, respectively. The heat pipe was kept horizontal during the whole test operation.

In most of the test runs, heat input was started from a low level, then was stepwise increased. To ensure the reproducibility of the heat pipe performance, tests were conducted also in stepwise decrease of the heat input after tests at higher heat input levels were made. This was done in Runs 1 and 4 of single-component test, and in Run 11 of gas-loaded test. In Run 13, tests with the same heat input level were conducted at a different date. The results showed that the performance of present heat pipe system was reproducible, and the hysteresis effect which often existed in pool boiling and wick boiling systems did not exert any noticeable influence on the overall heat pipe performance.

RESULTS AND DISCUSSION

The thermal conductance of the liquid-saturated wick

The thermal conductance of the liquid-saturated wick is an unknown property which can be determined accurately only by experiments. While phase change occurs in the evaporator wick of some existing heat pipe systems [8, 9], it is doubtful that the wick conductance can be evaluated meaningfully from the wick

vaporization characteristics. In the condenser section, phase change is unlikely to occur inside the wick. Furthermore, it was shown that convection caused by the flow of condensate is generally negligible [4]. Therefore, the thermal conductance of the liquid-saturated wick can be determined from the performance of the heat output section by the conduction equation

$$k_i = \frac{Q \ln (D_i/D_v)}{2\pi L_c (T_s - \bar{T}_{wc})} \tag{37}$$

where $\bar{T}_{wc}$ is the average wall temperature of the heat output section.

Strictly speaking, equation (37) is applicable for the case of condenser section identical to the heat output section under the steady-state condition that all the heat input takes part in the vaporization–condensation process. In the actual case, the effect of axial wall conduction causes the condenser section longer than the heat output section. Therefore, to evaluate k_i, it is necessary to obtain $\bar{T}_{wc}$ equivalent to that for the case of no axial wall conduction.

In the present experimental Runs 1, 2, 4 and 7, the heat output section is so long that the axial conduction effect is localized in the vicinity of the junction of the adiabatic and heat output sections. In these cases, $\bar{T}_{wc}$ is practically represented by the condenser wall temperature excluding the region influenced by axial wall conduction. In Runs 3 and 6, the heat output section is relatively short. The effect of axial wall conduction is so pronounced that the condenser lengths determined from the wall temperature profiles are respectively 54 per cent and 96 per cent longer than the heat output sections. To determine $\bar{T}_{wc}$ from the wall temperature vs length plot, such as the one shown in Fig. 1, the area beneath the vapor temperature is reshaped into a rectangle with length equal to the length of the heat output section. Thus, the width of the rectangle is equal to $T_s - \bar{T}_{wc}$. In Run 5, the wall temperature decreases monotonically from the evaporator to the condenser, indicating that there is heat conduction from the evaporator directly to the condenser through the pipe wall. In this particular case, not all the heat input takes part in the condensation process. Therefore, equation (37) is not applicable.

Figure 5, which depicts the variation of heat flux with temperature difference across the wick in the heat output section, $T_s - \bar{T}_{wc}$, shows that the data obtained under a wide range of heat input conditions and different geometries fall almost on straight lines. The wick thermal conductance, determined from the best fit lines and equation (37), yields the values of 0·0218 W/cm°C for the water-saturated wick and 0·00929 W/cm°C for the acetone-saturated wick. The result of this evaluation not only gives the values of the wick conductance, which provides a basis for wall temperature calculations, but also confirms the assumption that radial conduction is the governing heat-transfer mode in the condenser wick.

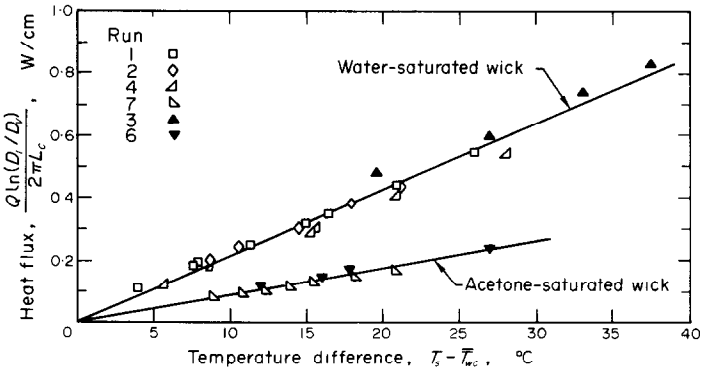

FIG. 5. Thermal performance of the heat output sections.

The effect of phase change in the evaporator wick

The present dimensionless analysis for single-component heat pipes implies that, by using the vapor temperature as a datum, the wall temperature profiles can be normalized by a scaling factor. This factor is the temperature drop across the evaporator wick under the condition that all the heat input is conducted radially through the evaporator wick. Therefore, before establishing the validity of the analytical prediction, it is necessary to correlate the data at different heat input conditions in dimensionless forms.

Figures 6–10 depict typically the variation of dimensionless wall temperature profiles along the heat pipe tested under different levels of heat input, in four distinct arrangements of heat pipe geometry, and with

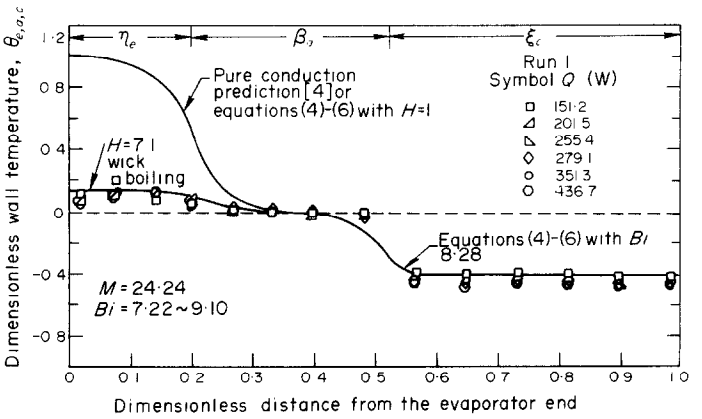

FIG. 6. Comparison of predicted wall temperature profile with the experimental data of Run 1.

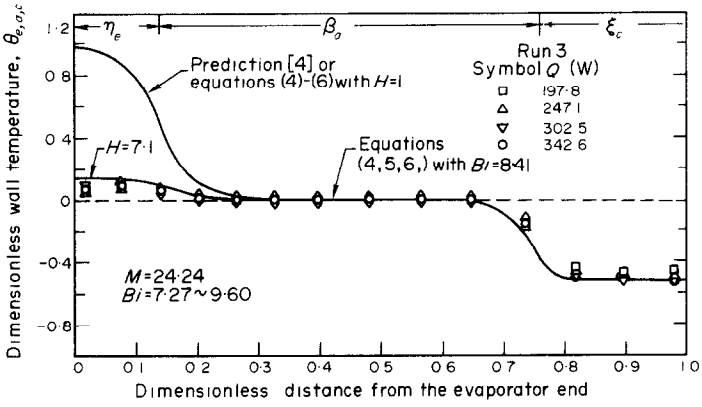

FIG. 7. Comparison of predicted wall temperature profile with the experimental data of Run 3.

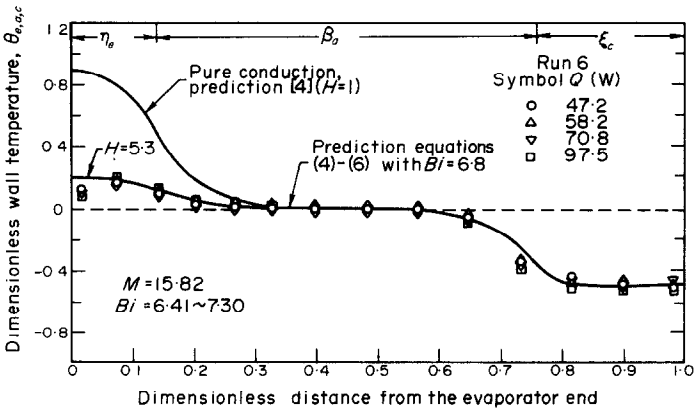

FIG. 8. Comparison of predicted wall temperature profile with the experimental data of Run 6.

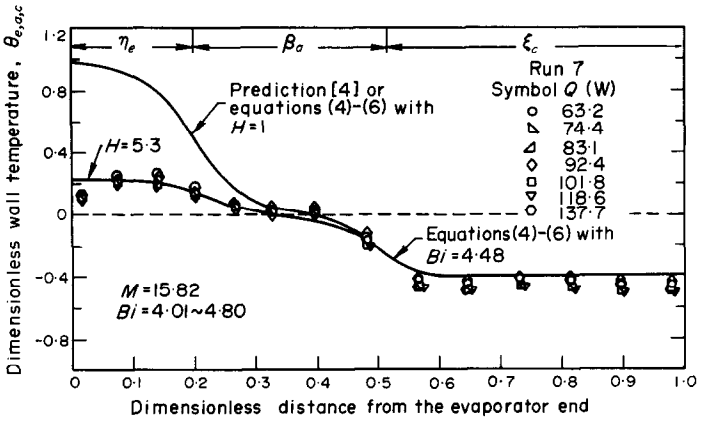

FIG. 9. Comparison of predicted wall temperature profile with the experimental data of Run 7.

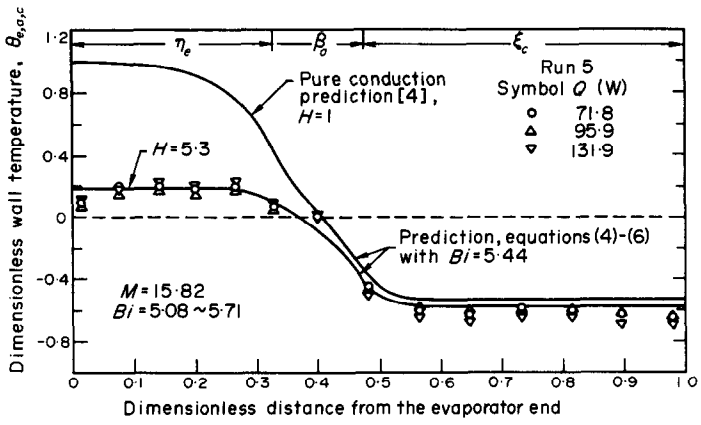

FIG. 10. Comparison of predicted wall temperature profile with the experimental data of Run 5.

two different working fluids (water and acetone). It is shown that the data are correlated very well in the appropriate dimensionless forms. The comparison of the correlated data with the prediction for $H = 1$, which corresponds to the case of pure conduction across the evaporator wick [4], indicates that phase change phenomenon occurs inside the evaporator wick that results in a temperature drop smaller than that of conduction.

In Figs. 6–10, the data from the water and acetone heat pipes agree very well with the predicted wall temperature profiles with $H = 7{\cdot}1$ and $5{\cdot}3$ respectively. This indicates that the effective conductance of the evaporator wicks for water and acetone heat pipes are respectively, $7{\cdot}1$ and $5{\cdot}3$ times its corresponding liquid-saturated wick conductance. For heat pipes with short heat input sections, as shown in Fig. 7, the pronounced axial conduction effect for the cases of $H = 1$ is shown to be largely subdued by the existence of phase change. This is due to the fact that phase change inside the wick increases substantially the contribution of radial heat flux across the wick as compared to axial conduction along the pipe wall. The parameter M, which governs the effect of axial conduction and is defined by equation (2), is increased by a factor of $H^{1/2}$ for the heat input section.

In Figs. 6–8, the convergence of the predicted temperature profiles and the curves for $H = 1$ at the adiabatic sections show that phase change in the evaporator exerts practically no effect on the vapor and condenser wall temperatures for heat pipes with long adiabatic sections. For heat pipes with shorter adiabatic sections, such as the one shown in Fig. 9, the axial conduction effect for the $H = 1$ curve indicates

that there is direct heat transfer from the evaporator to the ambient through the pipe wall. However, the direct heat transfer is eliminated as the axial conduction effect is subdued by the existence of phase change in the evaporator wick. For heat pipes with very short or no adiabatic sections, as shown in Fig. 10, the effect of axial conduction is so pronounced that the "adiabatic section" is essentially non-existent. In this case, the phase change in the evaporator decreases the amount of energy conducted axially along the wall, thus increasing the vapor temperature and the temperature drop across the condenser wick.

Among the existing studies of wick vaporization characteristics, reported heat-transfer mechanisms include pure conduction [4, 6, 7, 13], nucleate boiling and ebullition [6, 8, 9, 14–16], film boiling [17], meniscus receding [8, 18] and vapor blanketing [19], etc. It is difficult to ascertain the cause of these phenomena. However, it is apparent from the present result of $H = 7{\cdot}1$ and $5{\cdot}3$ for the water and acetone heat pipes that nucleate boiling or partial saturation exists in the present heat pipe system. To compare the present H values with those from the reported heat pipe studies is difficult, since the thermal conductances of the wicks used in the specific tests are not known. Studies of wick boiling [8, 9, 13, 14, 20] show that nucleation is observed at very low wall superheat and the heat-transfer coefficient for wick boiling can be as high as ten times that for pool boiling from a bare surface [20]. This implies that H can be an order of magnitude larger than one. For those studies with measured overall wall temperature profiles, the H values can be estimated from the wall temperature vs length plot. By dividing the area beneath the vapor temperature by that above it, the H value is approximately equal to one for Holm and Miller's model heat pipe [21], Schwartz [22], and Sockalingam [6], 2·5 for Tien and Rohani [23], and 2·0 and 5·0 for Neal [24]. While no general conclusion can be drawn to satisfy the performance of all the existing heat pipes, it is apparent from the existing results that the heat-transfer mechanism in the evaporator wick depends on the structure and surface condition of the wick and wall as well as the properties of the working fluid.

The effect of non-condensible gas

When non-condensible gas exists inside an operating heat pipe, it is swept by the vapor flow to the condenser end, forming an inert zone in the heat output section. This non-condensible gas region decreases the effective length of the heat output section thus increasing the vapor temperature and the overall temperature drop along the heat pipe. While a heat pipe operates with a small external heat-transfer coefficient, the existence of non-condensible gas can be detected by a sharp drop of wall temperature near the condenser end [5, 11]. However, this is not the case for a heat pipe which operates with a large external heat-transfer coefficient. Indeed, it will be shown that the condenser wall temperature does not vary appreciably with the amount of non-condensible gas.

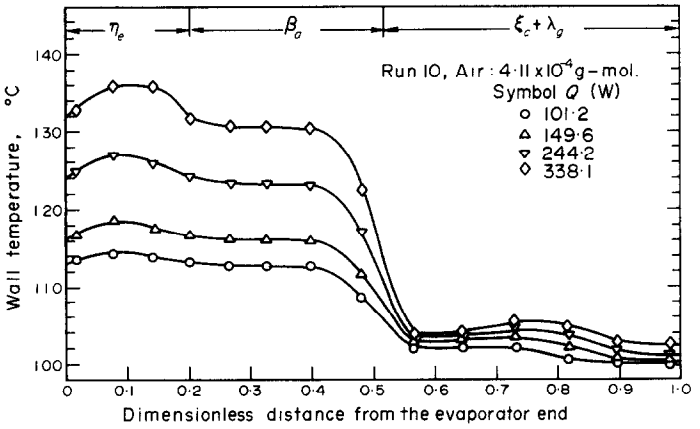

FIG. 11. Wall temperature profiles of a gas-loaded water heat pipe with 10 cm^3 of air.

While detailed test data are given in [12], only typical cases will be presented to demonstrate the effect of non-condensible gas and heat input to the heat pipe. Figure 11 shows the variation of wall temperature along the heat pipe with 10 cm^3 of air. It is noted that the temperature profiles appear to be similar to those of single-component heat pipes. The difference between the areas above and beneath the vapor temperature lines could be easily mistaken as the occurrence of phase

change in the evaporator wick. However, when the vapor and gas temperatures are measured, as illustrated in Fig. 12, the effect of non-condensible gas becomes evident. At lower levels of heat input, the vapor temperatures drop to the ambient temperature near the condenser end, indicating that the end portion of the heat pipe is completely inactive. At higher levels of heat input, the non-condensible gas is pushed to a narrower region in the condenser end. The combined effect of axial conduction and gas diffusion causes the vapor to penetrate into the non-condensible gas region, and thus raises the temperature higher than the ambient. In Fig. 12, the sudden drop of temperature indicates that the interface is sensitive to the condition of ambient environment which is generally constant within $\pm 0{\cdot}5°C$ and to the heat source which generally fluctuates by ± 2 per cent during the tests.

Figure 15 is a typical cross-plot of wall temperature profiles with different amounts of non-condensible gas and at constant heat input. It shows that the amount of non-condensible gas does not have an appreciable influence on the condenser wall temperature. On the other hand, the evaporator wall temperature is substantially increased with non-condensible gas. This behavior is in contrast to cases of heat pipes operating with small external heat-transfer coefficient [5, 11], in

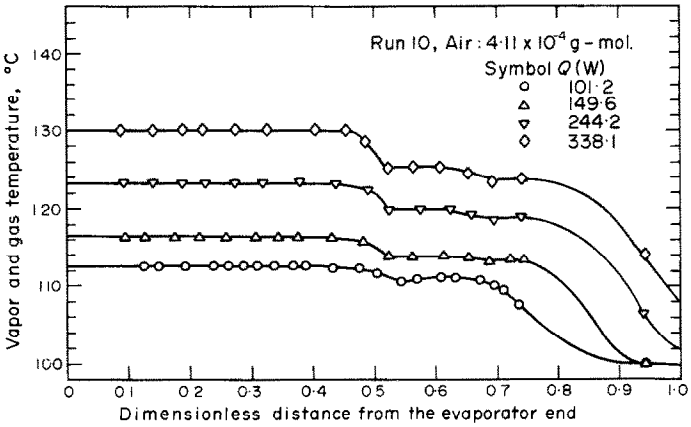

FIG. 12. Vapor and gas temperature profiles of a gas-loaded water heat pipe with 10 cm^3 of air.

near the location of dimensionless distance 0·52 from the evaporator end is believed to be caused by aluminum flanges which act like effective cooling sinks at the junction of adiabatic and heat output sections. This phenomenon becomes less pronounced with larger amounts of non-condensible gas.

Similar to the case presented in Figs. 11 and 12, Figs. 13 and 14 depict the variation of wall and vapor temperature profiles along the heat pipe which contains 70 cm^3 of air. It is shown that, with large amounts of non-condensible gas, the vapor and gas temperatures always drop to the ambient temperature at present range of heat input.

Fluctuations of vapor temperature were noticed in the region of the vapor and gas interface in several runs. Generally, the fluctuations become more pronounced with larger amounts of non-condensible gas and at higher levels of heat input. The worst case, shown in Fig. 14, amounts to $\pm 0{\cdot}8°C$. This probably which the evaporator wall temperatures are relatively insensitive to the amount of non-condensible gas while the condenser wall temperatures vary substantially. Figure 16 shows the vapor and gas temperature profiles corresponding to those given in Fig. 15. The effect of non-condensible gas becomes manifest. When there is no non-condensible gas, the vapor temperature is constant. As the amount of non-condensible gas increases, the inactive portion of the heat output section increases, and so does the pure vapor temperature in the evaporator end.

With the vapor and gas temperature profiles given, it is of interest to compare the known gas inventory in the pipe with those calculated by integrating equation (35). The result, which is shown in Table 1, indicates a good agreement in general, but deviates at high heat-input levels. This discrepancy is partly due to the sudden temperature drop near the region in contact with the aluminum flange. In addition, at high

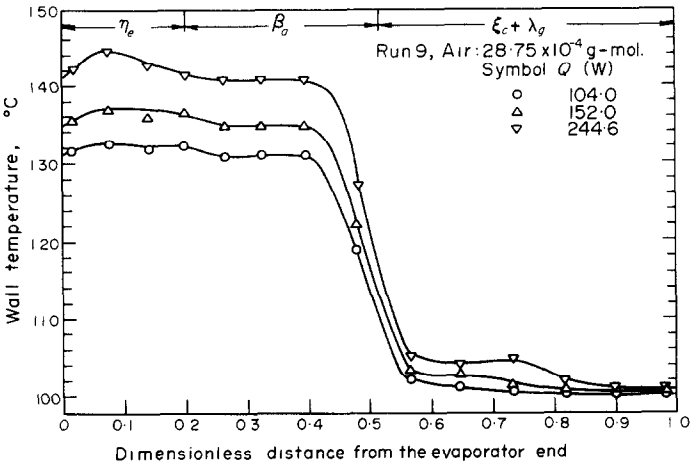

FIG. 13. Wall temperature profiles of a gas-loaded water heat pipe with 70 cm³ of air.

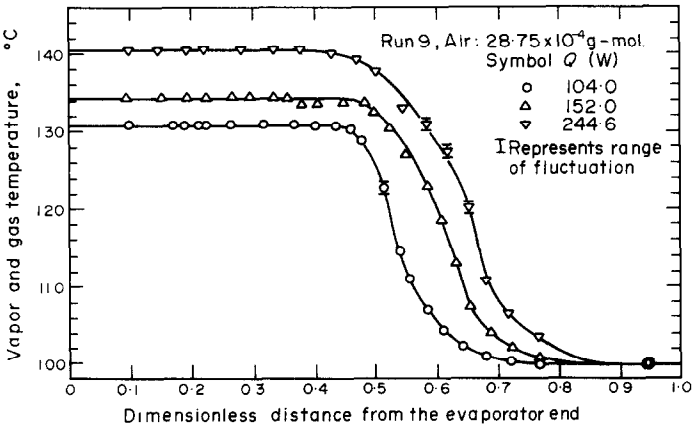

FIG. 14. Vapor and gas temperature profiles of a gas-loaded water heat pipe with 70 cm³ of air.

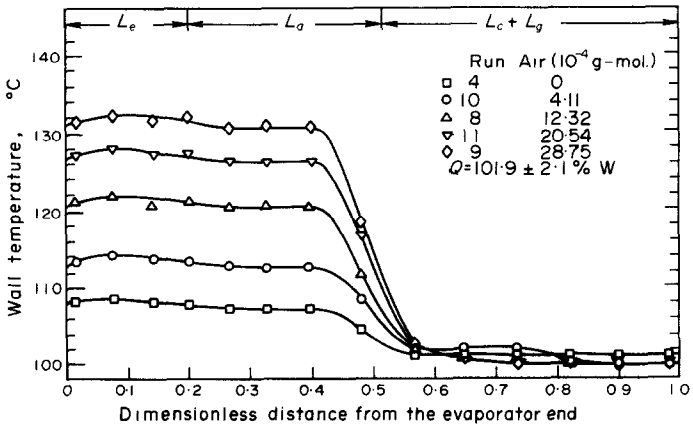

FIG. 15. The effect of non-condensible gas on the wall temperature profiles of a gas-loaded water heat pipe.

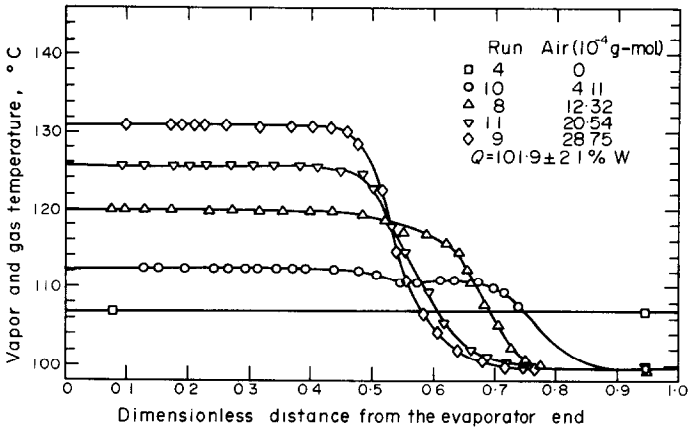

FIG. 16. The effect of non-condensible gas on the vapor and gas temperature profiles of a gas-loaded water heat pipe.

Table 1. Tabulation of L_g for the gas-loaded-water heat pipes

Run No.	Q (W)	N (10^{-4} g-mol) Measured	N (10^{-4} g-mol) Calculated by equation (35)	T_s (°C)	T_{gL} (°C)	L_g (cm)	λ_g (L_g/L)
8	101·8	12·32	12·6	120·1	99·7	21·10	0·346
8	150·4	12·32	12·1	123·3	99·8	17·57	0·288
8	250·0	12·32	19·1	130·2	99·8	12·31	0·202
8	335·9	12·32	19·4	136·2	103·0 ±1·0	9·96 ±0·40	0·163 ±0·007
9	104·2	28·75	28·9	130·8	99·8	27·82	0·456
9	152·0	28·75	29·8	134·5	99·8	23·57	0·386
9	244·6	28·75	38·0	140·5	99·8	18·38	0·301
10	101·2	4·11	5·7	112·6	99·8	12·68	0·208
10	149·6	4·11	5·8	116·4	100·0	9·32	0·153
10	244·2	4·11	7·4	123·3	104·4 ±1·0	6·99 ±0·28	0·115 ±0·005
10	338·1	4·11	9·5	130·1	111·0 ±1·0	5·90 ±0·24	0·097 ±0·004
11	100·8	20·54	21·2	125·8	99·8	25·47	0·417
11	150·8	20·54	22·9	129·1	99·8	21·48	0·352
11	240·7	20·54	25·8	135·1	99·8	16·35	0·268
11	347·3	20·54	31·2	141·8	99·8	12·55	0·206

heat-input levels, the heat-transfer rate and the vapor flow rate are probably large enough that the temperature variation in the radial direction is not negligible as compared to the vapor temperature drop along the heat pipe. Since the definition of L_g is dependent only on the end conditions, instead of the whole temperature profile, the measured N values will be used in the later calculations.

Figure 17 compiles the data given in Figs. 11–14 into dimensionless forms. The data of $Q = 244{\cdot}2$ W in Run 9 are excluded because of overlapping with other data. The saturated vapor temperatures used in the calculation of dimensionless wall temperatures are the pure vapor temperatures measured near the evaporator end. It is shown that, with the presence of non-condensible gas, the condenser wall temperature at different levels of heat input cannot be correlated by the dimensionless parameters which apply to the single-component heat pipes. The wall temperatures of the heat input and part of the adiabatic sections correlate well, indicating that the non-condensible gas exerts little influence on the heat-transfer characteristics of vaporization. The difference between the prediction of single-component cases and the present data becomes more pronounced

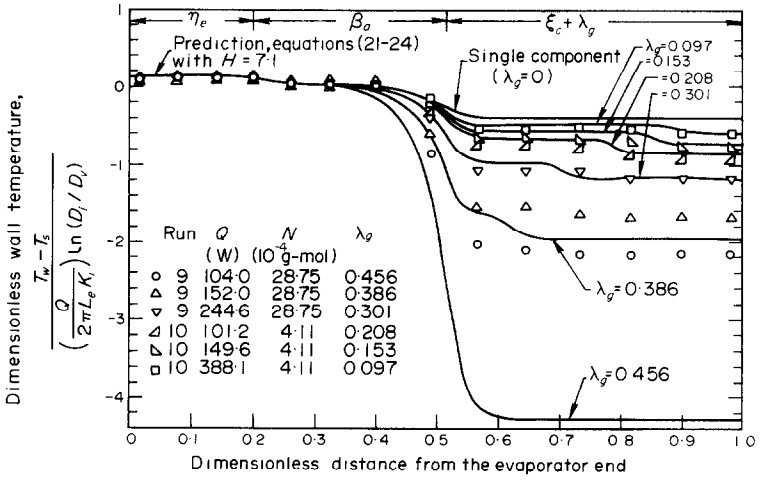

FIG. 17. Dimensionless wall temperature profiles of gas-loaded water heat pipes with different dimensionless lengths for the non-condensible gas region.

when the length of the non-condensible gas region is longer. To compare the wall temperature data shown in Fig. 17 with analytical predictions, it is necessary first to evaluate the length, L_g, that characterizes the non-condensible gas region.

The length for the non-condensible gas region

To evaluate the length, L_g, requires the measurement of vapor temperature at the two ends of heat pipe, i.e. the pure vapor temperature at the evaporator end, T_s, and the temperature of the non-condensible gas or the partially saturated vapor at the condenser end, T_{gL}. In the present test, the vapor temperature measured closest to the condenser end is at dimensionless distance 0·938 (i.e. 1·5 in from the end flange). For those runs in which the vapor temperature does not drop to the ambient temperature at this location, T_{gL} can only be obtained by extrapolation. Therefore, uncertainties are involved in the determination of L_g.

Tabulated in Table 1 are the values of L_g for gas-loaded water heat pipes. There are three cases associated with ± 4 per cent uncertainty. For gas-loaded acetone heat pipes, uncertainties are involved for all the sixteen cases, in which most of the uncertainties are above 50 per cent. The data for acetone heat pipes are, therefore, not included here.

The data given in Table 1 show that L_g decreases with the amount of non-condensible gas, N, but not linearly as indicated in equation (36). The values of L_g also appear to vary with the heat input. For a fixed heat pipe geometry, an increase in heat input causes an increase in vapor temperature and a corresponding larger increase in P_{gL} as the vapor pressure increases, thus causing L_g to decrease. For the present test range, the data of L_g appear to be well correlated by a single curve, which is

$$\frac{L_g}{L - L_e - L_a} = 1 - 0{\cdot}932 \exp\left(-0{\cdot}0937 \frac{N}{Q}\right) \quad (38)$$

for $1{\cdot}22 \leqslant N/Q \leqslant 27{\cdot}59$, where N/Q has the units of 10^{-6} g mol/W. It should be noted that equation (38) is only applicable to the present heat pipe system.

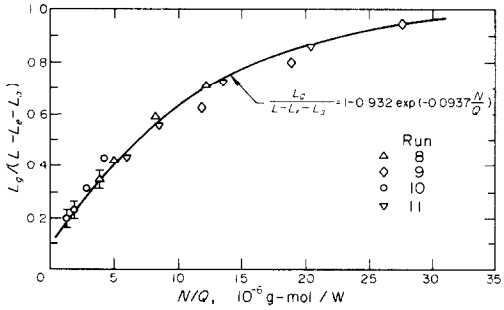

FIG. 18. Correlation of the length for the non-condensible gas region with the heat input level and the amount of non-condensible gas for the present heat pipe system.

With L_g known, the wall temperature profile of a gas-loaded heat pipe can be calculated by equations (21)–(24). Calculations for Runs 9 and 10 are compared with experimental data in Fig. 17. It is shown that the prediction of temperature drop in the heat output section is much too large for $\lambda_g = 0{\cdot}456$, 20 per cent too large for $\lambda_g = 0{\cdot}386$, and agrees well with cases for smaller

λ_g's. The large discrepancy at $L_g \rightarrow (L_g + L_c)$ is difficult to ascertain, since the condenser length, L_c, which governs the temperature drop at the heat output section is very sensitive to experimentally determined L_g values. For instance, 6 per cent decrease due to correction of inaccuracy in the determination of $\lambda_g =$ 0·456 will increase L_c by 100 per cent, thus resulting in reduction of temperature drop by 31 per cent. Another possible source of error could be caused by neglecting mass diffusion, which results in more axial heat conduction and consequently larger temperature drop.

CONCLUSIONS

The results obtained in the present study lead to the following conclusions:

1. A heat pipe is able to operate normally with phase change occurring inside the evaporator wick. The wick vaporization characteristics can be represented by an effective film coefficient which varies with different working fluids as well as the structure and surface condition of the wick and pipe wall, but are independent of the non-condensible gas in the heat output section.

2. While various heat-transfer mechanisms can exist in the evaporator wicks of different heat pipes, the heat-transfer mechanism in the condenser wick is governed by thermal conduction. The thermal conductance evaluated in the present study yields the value of 0·0218 W/cm°C for the water-saturated wick and 0·00929 W/cm°C for the acetone-saturated wick.

3. The thermal performance of a gas-loaded heat pipe is very sensitive to the condenser environment. For heat pipes operating with a large external heat-transfer coefficient, such as heat rejection by boiling, the amount of non-condensible gas has little effect on the condenser wall temperature. This is in contrast to cases of heat pipes operating with a small external heat-transfer coefficient, such as heat rejection by free convection or radiation, in which the condenser wall temperature drops sharply with non-condensible gas.

4. The effect of non-condensible gas can be characterized by a length parameter defined as

$$L_g \equiv \frac{R_u T_{gL} N}{A_v P_{gL}}$$

which varies with the heat input. An increase in heat input causes an increase in vapor temperature T_{gL}, and a corresponding larger increase in P_{gL} as the vapor pressure increases, thus causing L_g to decrease.

5. The effect of axial wall conduction becomes less pronounced with phase change in the evaporator wick, and more pronounced with non-condensible gas. In the former case, the phase change increases substantially the relative contribution of radial heat flux across the wick as compared to axial conduction along pipe wall. Therefore, the effect of axial wall conduction in the evaporator section is subdued. In the latter case, the non-condensible gas causes additional temperature drop in the condenser section, thereby increasing axial wall conduction in the condenser section.

6. The simple conduction model developed by Sun and Tien can be extended to include the phenomena of phase change inside the evaporator wick and the non-condensible gas by incorporating a dimensionless parameter which compares the effective film coefficient of the evaporator wick with that of pure conduction and the dimensionless length defined to characterize the non-condensible gas region.

REFERENCES

1. G. M. Grover, T. P. Cotter and G. F. Erickson, Structures of very high thermal conductance, *J. Appl. Phys.* **35**, 196–212 (1964).
2. E. R. F. Winter and W. O. Barsch, The heat pipe, in *Advances in Heat Transfer*, edited by T. F. Irvine and J. P. Harnett, Vol. 7, pp. 219–320. Academic Press, New York (1971).
3. C. L. Tien (editor), *Heat Pipes*, AIAA Selected Reprint Series, Vol. 16. Amer. Inst. Aeronautics and Astronautics, New York (1973).
4. K. H. Sun and C. L. Tien, Simple conduction model for theoretical steady-state heat pipe performance, *AIAA Jl* **10**. 1051–1057 (1972).
5. D. K. Edwards and B. D. Marcus, Heat and mass transfer in the vicinity of the vapor–gas front in a gas-loaded heat pipe, *J. Heat Transfer* **94C**, 155–162 (1972).
6. K. C. Sockalingam, Performance characteristics and optimization of water heat pipes, Ph.D. Thesis, Dept. of Nuclear Engineering, Univ. of California, Berkeley (September 1972).
7. J. K. Ferrell and H. R. Johnson, The mechanism of heat transfer in the evaporator zone of a heat pipe, A.S.M.E. Paper No. 70-HT/Spt-12 (1970).
8. R. A. Seban and A. Abhat, Steady and maximum evaporation from screen wicks, A.S.M.E. Paper No. 71-WA/HT-12 (1971).
9. J. C. Corman and G. E. Walmet, Vaporization from capillary wick structure, A.S.M.E. Paper No. 71-HT-35 (1971).
10. B. D. Marcus and G. L. Fleischman, Steady-state and transient performance of hot reservoir gas-controlled heat pipes, A.S.M.E. Paper No. 70-HT/Spt 11 (1970).
11. B. D. Marcus, Theory and design of variable conductance heat pipes, NASA CR-2018 (1972).
12. K. H. Sun, Thermal performance characteristics of heat pipes, Ph.D. Thesis, Dept. of Mechanical Engineering, Univ. of California, Berkeley (March 1973).
13. J. K. Ferrell and J. Alleavitch, Vaporization heat transfer in capillary wick structures, *Chem. Engng Symp. Ser.* **66**(102) (1970).
14. P. J. Marto and W. L. Mosteller, The effect of nucleate boiling on the operation of low temperature heat pipes, A.S.M.E. Paper No. 69-HT-24 (1969).
15. A. K. H. Abhat, Evaporation and nucleate boiling from heat pipe wicks, Ph.D. Thesis, Dept. of Mechanical Engineering, Univ. of California, Berkeley (September 1972).

16. A. Bähr, E. Bruck and W. Hufschmidt, Liquid–vapor interaction and evaporation in heat pipe, *2nd International Conference on Thermionic Electrical Power Generation* (1968).
17. K. G. Cartohers and R. D. Fox, Low temperature heat pipe performances near burnout conditions, presented at the *13th National Heat Transfer Conference*, A.I.Ch.E.–A.S.M.E., Denver, Colo. (August 1972).
18. K. R. Chun, Some experiments on screen wick dry-out limits, *J. Heat Transfer* **94C**, 46–51 (1972).
19. R. A. Moss and A. J. Kelly, Neutron radiographic study of limiting planer heat pipe performance, *Int. J. Heat Mass Transfer* **13**, 491–502 (1970).
20. P. S. O'Neil, C. F. Gottzman and J. W. Terbot, Novel heat exchanger increases cascade cycle efficiency for natural gas liquefaction, presented at the *Heat Transfer Symposium 68th National Meeting*, A.I.Ch.E. Houston, Texas, 28 February–4 March (1971).
21. F. W. Holm and P. L. Miller, Thermal scale modeling of a heat pipe, A.S.M.E. Paper No. 70-HT/Spt-14 (1970).
22. J. Schwartz, Performance map of the water heat pipe and the phenomenon of non-condensible gas generation, A.S.M.E. Paper No. 69-HT-15 (1969).
23. C. L. Tien and A. R. Rohani, Theory of two-component heat pipes, *J. Heat Transfer* **94C**, 479–484 (1972).
24. L. G. Neal, An analytical and experimental study of heat pipes, Report No. 99900-6114-R000, TRW Systems, One Space Park, Redondo Beach, Ca. (January 1967).